THE ASTROPHYSICAL JOURNAL, 414:345–356, 1993 September 1

DYNAMICS OF THE SOLAR CHROMOSPHERE. I. LONG-PERIOD NETWORK OSCILLATIONS

B. W. LITES,[1] R. J. RUTTEN,[2] AND W. KALKOFEN[3]
Received 1992 August 10; accepted 1993 March 9

ABSTRACT

We analyze differences in solar oscillations between the chromospheric network and internetwork regions from a 1 hr sequence of spectrograms of a quiet region near disk center. The spectrograms contain Ca II H, Ca I 422.7 nm, and various Fe I blends in the Ca II H wing. They permit vertical tracing of oscillations throughout the photosphere and into the low chromosphere. We find that the rms amplitude of Ca II H line center Doppler fluctuations is ~ 1.5 km s^{-1} for both network and internetwork, but that the character of the oscillations differs markedly in these two regions. Within internetwork areas the chromospheric velocity power spectrum is dominated by oscillations with frequencies at and above the acoustic cutoff frequency. They are well correlated with the oscillations in the underlying photosphere, but they are much reduced in the network. In contrast, the network Ca II H line center velocity and intensity power spectra are dominated by low-frequency oscillations with periods of 5–20 minutes. Their signature is much clearer in our Ca II H line center measurements than in previously used diagnostics which are contaminated by signals from deeper layers. We find that these long-period oscillations are not correlated with underlying photospheric disturbances, and we discuss their nature.

Subject headings: Sun: chromosphere — Sun: oscillations

1. INTRODUCTION

The nature of the mechanism(s) responsible for heating the solar chromosphere still eludes identification. It is not clear whether different mechanisms dominate in magnetic and nonmagnetic regions, to what extent chromospheric and coronal heating are related, whether chromospheric heating depends causally and locally on specific dynamical processes in the underlying photosphere and convection zone, or even whether the chromosphere is bifurcated into hot and cool domains with large temperature contrast. The fine structure and the dynamic behavior of the solar chromosphere imply that such issues are best addressed through observations with high spatial and temporal resolution. In particular, the linkage of chromospheric heating to small-scale dynamical phenomena is suggested by the ubiquity of sonic or near-sonic velocities inferred from both the widths of chromospheric lines and spatially resolved Doppler motions. This paper is the first in a series addressing such phenomena in the context of chromospheric energy balance.

There is much current interest in the dynamics of the magnetic elements that together constitute the magnetic network since these small-scale, strong field elements may harbor mechanisms by which energy is channeled from subsurface layers and the photosphere to the transition region and corona (see, e.g., reviews in Ulmschneider et al. 1991 and by Stenflo 1989). However, for all the theoretical work on flux tube properties and dynamics, there is a lack of observational insight into the dynamics of small-scale magnetic elements. We present new data on their oscillatory behavior, using the Ca II network as proxy for the magnetic network and the opaque core of the Ca II H line as our primary diagnostic.

The observations reported below were orginally intended as a search for high-frequency disturbances—periods below 1 minute—in the quiet Sun which, if present, should propagate upward in the solar atmosphere, turn into shocks, and dissipate acoustic energy in the low chromosphere in classical fashion (Biermann 1946; Schwarzschild 1948; review by Kuperus 1969). No conclusive evidence for the existence of such disturbances was found; the data have therefore not been published except for brief presentation in Lites (1985). However, in the course of a reanalysis prompted by interest in internetwork Ca II K_{2V} and H_{2V} grains (Rutten & Uitenbroek 1991), we found that the data display fundamental differences between the chromospheric dynamics of the Ca II network and of the internetwork.[4] Although such differences have been noted before (Orrall 1966; Title 1966; Liu & Sheeley 1971; Bhatnagar & Tanaka 1972; Giovanelli 1974, 1975; Damé, Gouttebrouze, & Malherbe 1984; von Uexküll et al. 1989; Deubner & Fleck 1990), the present observations yield clean diagnostics that show that the network contains low-frequency disturbances which are purely chromospheric and which are not excited by motions in the photosphere directly underneath.

The present series of papers may be regarded as a continuation of the earlier series called "High-Resolution Spectroscopy of the Disk Chromosphere" (Beckers et al. 1972; Wilson et al. 1972; Beckers & Artzner 1974; Cram 1974, 1978; Cram et al. 1977; Woods & Cram 1981; cf. Rutten & Uitenbroek 1991) since we employ similar Fourier analysis techniques to similar data. By separating a network and internetwork we extend the comparable lower atmosphere analyses of Lites, Chipman &

[1] High Altitude Observatory, National Center for Atmospheric Research, P.O. Box 3000, Boulder, CO 80307-3000.
[2] Sterrekundig Instituut, Postbus 80000, NL-3508 TA Utrecht, The Netherlands.
[3] Harvard-Smithsonian Center for Astrophysics, 60 Garden Street, Cambridge, MA 02138.

[4] We do not use the terms of *cell boundary* and *cell interior* to descibe network and nonnetwork; nor do we use *intranetwork*. Our motivation is that the Ca II network seen on Ca II K filtergrams and the magnetic network seen on high-resolution magnetograms are not characterized by mosaics of regularly shaped cells. Instead, they consist of irregular patterns made up by crinkled segments of variable lengths without the well-defined insides which using the terms *interior* and *intra* would imply.

White (1982) and Deubner & Fleck (1990) to chromospheric heights.

The organization of the paper is as follows. In § 2 we present the observations and their reduction. In § 3 we display time-resolved Ca II H spectra, Doppler measurements with their power spectra, and Fourier spectra of phase difference and phase coherence for various spectral features. All these measurements are split between network and internetwork. We compare our results with other work in § 4 and we draw conclusions in § 5.

2. OBSERVATIONS AND DATA REDUCTION

The observations discussed here (cf. Lites 1985) consist of a sequence of digital spectrograms obtained under good seeing conditions with the Vacuum Tower Telescope, echelle spectrograph and multidiode array (MDA) of the National Solar Observatory/Sacramento Peak. Simultaneous exposures of only 0.25 s duration were taken by two CCD cameras in two spectral windows, respectively, containing part of the Ca II H line ($\lambda = 396.85$ nm) and the core of the Ca I resonance line at $\lambda = 422.67$ nm. The wavelength sampling was $\Delta\lambda = 1.181$ pm pixel^{-1} for the Ca II window and $\Delta\lambda = 1.405$ pm pixel^{-1} for the Ca I region. The spectrograph slit had a width of 0".5 (0.4 Mm) and covered $\sim 78''$ (57 Mm) on the Sun, with 0".52 (0.38 Mm) per pixel. A single exposure is shown in Figure 1. The Ca II window ($\lambda = 396.63$–399.90 nm; *top*) contains the Ca II H core and inner blue wing, as well as several Fe I blends superposed on the latter. The Ca I window (422.62–422.70 nm; *bottom*) includes a medium-strong Fe I line at $\lambda = 422.64$ nm. Figure 1 and Table 1 specify the wavelengths and identifications of various lines and wing features used in this and the subsequent paper of this series.

The spectrogram sequence was obtained from 15:45 UT until 16:47 UT on 1984 April 12, close to the minimum of cycle 21. It has 5 s exposure cadence. A quiet region near disk center was tracked taking solar rotation into account. Previous experience has shown that the tracking is stable to $\sim 1''$ on the solar surface over durations of up to 1 hr.

Flat-field corrections were obtained following Lites et al. (1990) from spatially averaged spectrogram exposures taken before and after the spectrogram sequence, with the solar image put out of focus and slewed rapidly across the slit during exposure. Dark field exposures were also obtained before and after the spectrogram sequence. Linear temporal interpolations were applied to obtain pixel-by-pixel zero level and flat-field corrections. Additional spectrograms of the unfocused quiet Sun with a hairline in front of the slit served to coregister the two spectral windows onto the same spatial scale.

We have determined line center positions, line center intensities, wing intensities, and integrated intensities as specified in Figure 1 and Table 1 for each of the spectrograms in the sequence. The mean wavelength of three photospheric lines

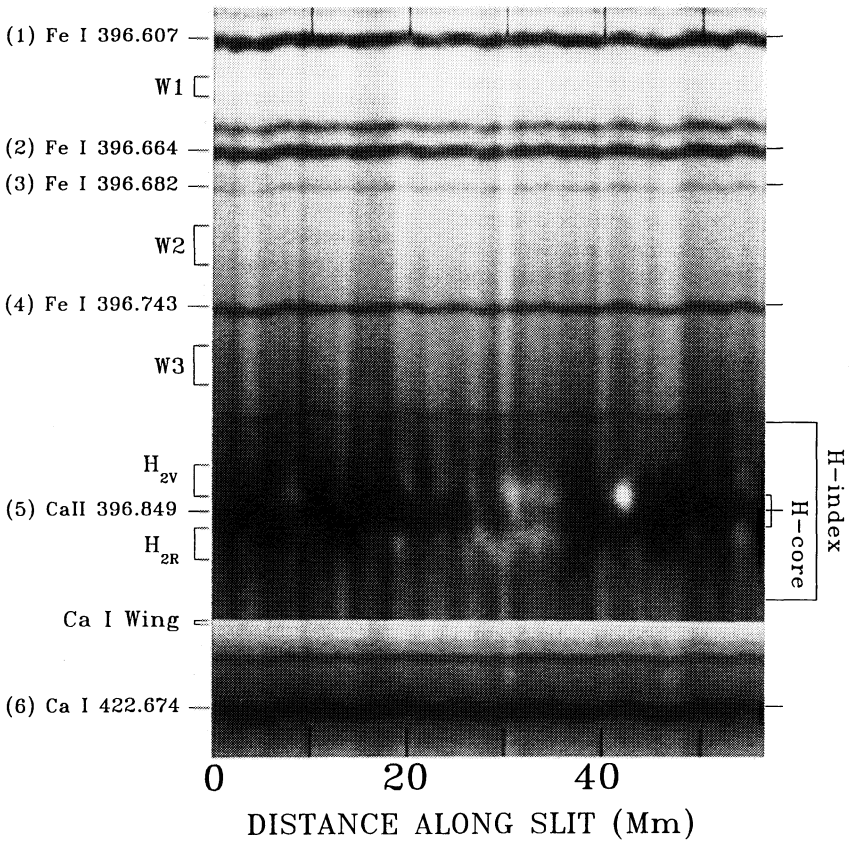

FIG. 1.—An individual spectrogram, taken 6.9 minutes from the start of the sequence, is shown. The abscissa is the spatial coordinate along the spectrograph slit, marked in Mm (1 Mm $\approx 1''.4$). The ordinate indicates wavelength in nanometers, increasing downward. The upper (larger) part is the Ca II H window; the lower part contains Ca I 422.67 nm. The numbers in parentheses designate the lines (specified in Table 1) for which line-center Doppler and intensity fluctuations have been measured. The bandwidths of the additional intensity measurements listed in Table 1 are also indicated. Note the bright network emission features (both Ca II H_{2V} and H_{2R}) in the middle of the spectrogram, and the bright internetwork H_{2V} grain near $x = 42$ Mm. The H wing contains bright and dark streaks called whiskers by Beckers & Artzner (1974). The Ca I and Fe I lines primarily display Dopplershifts. The slight spatial displacement between the two windows was corrected in the data reduction. The intensity scaling has been adapted to show the line core and wings simultaneously.

TABLE 1

PARAMETERS FOR OBSERVED LINES AND WING INTENSITIES

	LINES				WING INTENSITIES		
LINE NUMBER	Wavelength (nm)[a]	Transition	Multiplet	Formation Height[b] (km)	Central Wavelength (nm)	Range (nm)	Designation
1.....	Fe I 396.607	a^2F_5–$y^3D^o_7$	45	386	396.632	±0.005	W1
					396.632	±0.005	W1
2.....	Fe I 396.664	$z^5D^o_9$–f^5F_{11}	562	367			
3.....	Fe I 396.682	a^3D_5–$u^3G^o_7$	659	250[c]			
					396.713	±0.010	W2
4.....	Fe I 396.743	b^3H_9–$u^3G^o_7$	604	358			
					396.774	±0.010	W3
5.....	Ca II 396.849	$^2S_2$–$^2P^o_2$	1	1046	396.849	±0.045	H-line Index
					396.849	±0.008	H-line Core Intensity
					396.833	±0.008	H_{2V}
					396.865	±0.008	H_{2R}
6.....	Ca I 422.674	$^1S_1$–$^1P^o_3$	2	634	422.620	±0.010	Ca I Wing

[a] From Moore, Minnaert, & Houtgast 1966.

[b] Heights derived from phase delays measured at high frequencies (to be presented in Paper II of this series). Errors in these heights due to errors in measurement of the phase difference are of the order of 10%–20%, but the ordering of heights of formation among the lines is unambiguous.

[c] Line formed lowest: formation height estimated.

(Nos. 1, 2, and 4 of Table 1), each averaged along the entire length of the slit, was used to supply a wavelength reference for each exposure. Doppler shifts of the various lines were referenced to this frame-averaged wavelength reference in order to minimize the influence of spectrograph instabilities. We also used cross correlations of the spatial variations in the Ca II wing intensities between successive frames to partially compensate for seeing-induced guiding errors parallel to the slit.

We employed algorithms developed by Lites & Thomas (1985) to measure the *centers* of the absorption lines: the wavelength of minimum intensity after applying a numerical filter to reduce high-frequency noise. The wavelength of minimum intensity (the line center shift) is preferable to measures of the Doppler velocity extracted from the inner wings. Theoretical contribution functions indicate that the intensity at line center is usually emitted from a narrower height range than that of the line wings. Also, for lines that are sensitive to the granular overshoot layer, the line center contribution function varies less under the influence of granular motions than do the wing contribution functions (e.g., Bruls & Rutten 1992). In Paper II of this series we will demonstrate from oscillation phase analysis of the Fe I blends and the Ca I resonance line in our data that discrimination is indeed possible between line center heights of formation which differ by only a small fraction of a scale height. The results of that analysis are specified in Table 1 as mean heights of formation on a relative scale.

Measuring Doppler velocities in the Ca II resonance lines is more problematic due to the frequent occurrence of intensity reversals in their cores. The H_{2V} peak intensity is thought to be enhanced by the lack of blue wing opacity in overlying layers when the chromospheric material moves downward (e.g., Athay 1970; Liu & Skumanich 1974; Cram, Brown, & Beckers 1977; Mein et al. 1987). Rutten & Uitenbroek (1991) conclude that the H_{2V} over H_{2R} intensity ratio as plotted in the V/R diagram of Cram & Damé (1983) represents an indirect measure of line center (H_3) redshift. We measure both the H_{2V} emission strength and the H_3 wavelength, but show only the latter quantity in this paper. The two measures indeed show similar oscillatory phase behavior. We nevertheless caution the reader that neither may be a reliable indicator of true chromospheric velocities, due to their interrelation (see Lites 1992).

3. RESULTS

Figure 1 indicates that the spectrograph slit traversed a segment of the chromospheric network because there is enhanced emission in both the H_{2V} and H_{2R} features near $x = 30$ Mm. The other parts of the frame display typical internetwork behavior, with a bright H_{2V} grain at $x = 42$ Mm and with irregular whiskers extending into the wings. The dynamical behavior of the internetwork will be discussed in the next paper of this series. We concentrate here on the network segment.

3.1. *Time-resolved Spectra*

Figure 2 shows the temporal development of the spectrum in the Ca II window for four positions along the slit. This display is similar to the time-resolved spectra of Cram & Damé (1983). Intensity is plotted as gray scale. The spatial position along the slit is specified at the top of each panel (see Fig. 1). The inner two panels are representative of the calcium network, the outer two of the internetwork. The inferred Ca II H line center wavelength is indicated for each exposure by a small white dot. The good correspondence with the excursions of the dark H_3 feature demonstrates that this algorithm works properly.

The internetwork (outer panels) shows familiar oscillatory behavior, with rapid Doppler excursions, inner wing intensity variations and bright, sometimes repetitive H_{2V} grains (e.g., Cram & Damé 1983; Rutten & Uitenbroek 1991). The network pattern is strikingly different. The middle panels show much slower Ca II H Doppler excursions. Both the H_{2V} and H_{2R} features generally appear bright. H_{2V} is often bright while H_3 shifts to the red but, in contrast to the internetwork behavior, H_{2R} also brightens for H_3 blueshift. There are also moments of appreciable H_3 Dopplershift without much enhancement. There is no clear correspondence between the intensity modulation of the inner H-line wings and the H_3 behavior, again in contrast to the internetwork panels. Finally, there are patterns of tilted light and dark bands across the H-line core in the

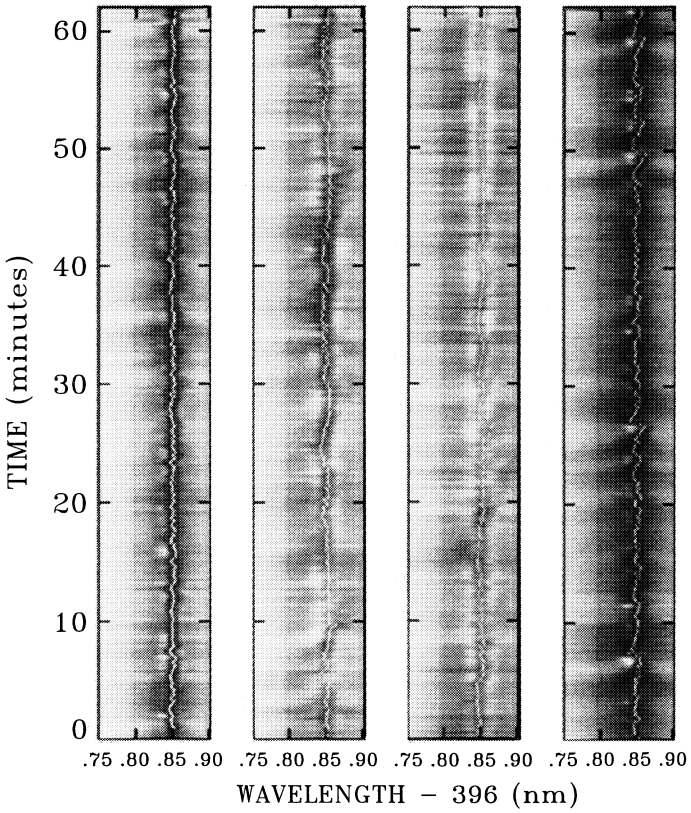

FIG. 2.—Time-resolved spectra of the Ca II H line are displayed for the four positions along the slit indicated at the top. From left to right: 9 Mm, 27 Mm, 30 Mm, and 43 Mm. Each panel shows spectrum intensity in the Ca II H window plotted in gray scale against wavelength, with time increasing upward. The superimposed dots indicate the measured position of Ca II H line center. The two middle panels are from the segment of network covered by the slit; the outer panels display internetwork behavior. The horizontal striping is produced by variations in atmospheric seeing. The H_{2V} grain in the right-hand panel is also seen in Fig. 1.

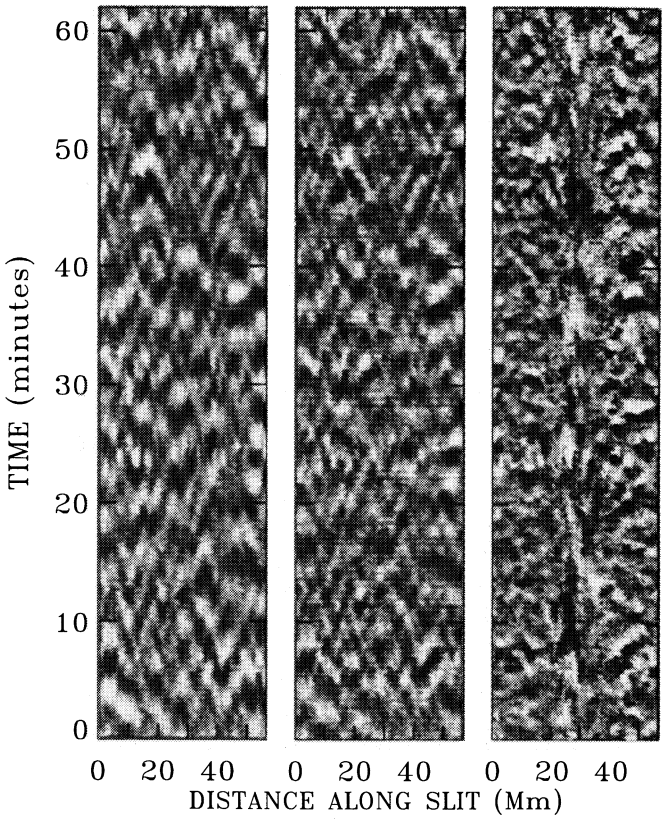

FIG. 3.—The gray scale plot shows the space-time behavior of the Doppler velocities measured from the three lines specified at the top of the panels. The gray scale coding has redshift dark, blueshift bright. The Fe I 396.682 nm line (*left*) is photospheric; the Ca I 422.674 nm line (*center*) originates in the temperature minimum region; the Ca II H line center (*right*) is chromospheric. The horizontal striping is due to seeing variations.

network panels which appear to mark progress from the blue to the red side of line center. These represent the spectral evolution of the slow oscillations discussed below.

3.2. *Doppler Measurements*

Figure 3 illustrates the space-time development of the Doppler velocities measured from a photospheric Fe I line (No. 3 of Table 1, left-hand panel), the Ca I resonance line which forms in the temperature minimum region, and the chromospheric Ca II H_3 feature (right-hand panel). The photospheric motions display the characteristic wavy band structure of the solar 5 minute oscillation, which is the dominant constituent of the Doppler excursions in the lower atmosphere. It produces apparent zig-zag patterns from the complex interference among the solar *p*-modes. Their slopes in the left-hand panel imply horizontal phase speeds of 30–100 km s^{-1} with a characteristic size of 3–10 Mm (cf. Musman & Rust 1970).

The velocity signature from the temperature minimum (middle panel) is similar. The characteristic periods and horizontal sizes of the interference pattern are somewhat smaller because high-frequency oscillations gain importance at larger heights (e.g., Evans et al. 1963; Noyes & Leighton 1963; Orrall 1966; Noyes 1967; Frazier 1968; Cram 1978). Qualitatively, however, the patterns in the first and second panels are the same. The brightest and darkest spots marking large Doppler excursions correlate well between the two panels. In neither panel does one discern the presence of network around $x = 30$ Mm.

The right-hand panel shows that the Ca II H_3 excursions differ markedly from those in the lower atmosphere. The presence of network in the middle of the panel is quite clear from its striking difference in behavior with the adjacent internetwork. The latter contains large-amplitude 3 minute oscillations, especially at the right, with large redshifts (dark) often followed quickly by large blueshifts (bright). The internetwork patterns are correlated with the *p*-mode patterns in the other panels, but this correlation is not very obvious due to mixing of 5- and 3-minute oscillations. In contrast, much longer periods dominate in the network. The middle of the panel ($x = 25$–35 Mm) shows far slower modulation, producing patterns of near-vertical, narrow bright, and dark streaks rather than roundish dots. The *p*-mode zig-zag patterns are even less prominent, if present at all.

3.3. *Power Spectra*

Figure 4 presents spatially resolved velocity power spectra plotted in gray-scale coding as a function of position along the slit. For reference, the top panel displays the time-averaged spectral profiles of Ca II H, also as gray-scale versus spatial position along the slit. It clearly shows the presence of network for $x = 25$–35 Mm in the form of bright H_{2V} and H_{2R} emission.

The two lower panels display velocity power spectra of Ca II H_3 (middle) and Fe I 396.682 nm (bottom). Each column rep-

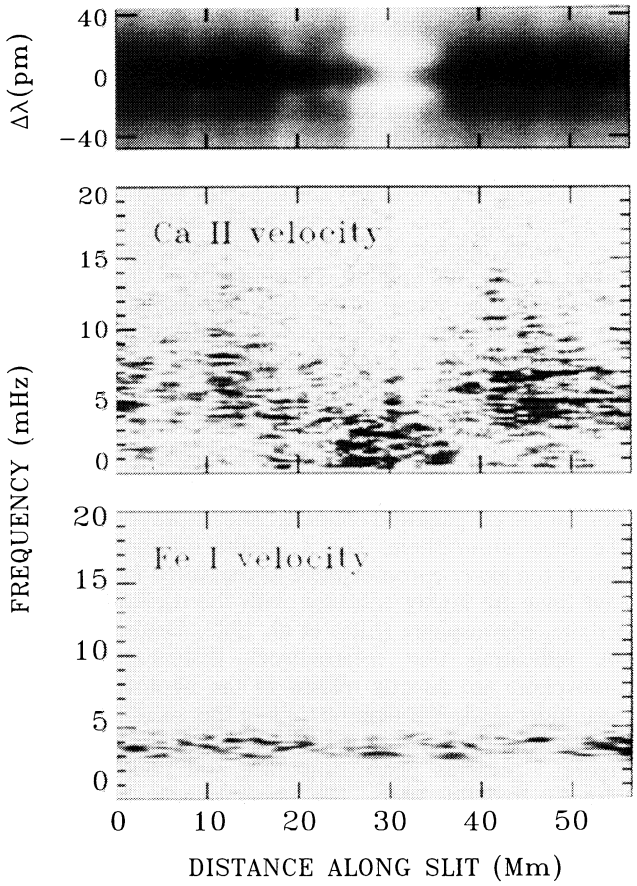

FIG. 4.—The top panel displays the time-averaged Ca II H profile as a function of spatial position. The bright K_2 bands in the middle reveal the segment of network covered by the slit. The middle and bottom panels show the power in the Doppler velocity fluctuations of Ca II H_3 and Fe I 396.682 nm, respectively, as a function of frequency of oscillation and spatial position along the slit. Darker gray-scale shading corresponds to higher power in the bottom two panels. These and subsequent power spectra are presented only out to $f = 20$ mHz, whereas the Nyquist frequency is at $f = 100$ mHz. However, all power spectra are featureless at the frequencies not shown.

resents a temporal power spectrum for the corresponding 0.4 Mm pixel width along the slit. The two panels are very different. The Fe I power spectra in the bottom panel show no clear distinction between network and internetwork. In contrast, the Ca II power spectra in the middle panel differ very markedly between these two regions. The network segment at $x = 25$–35 Mm (top panel) corresponds closely to the presence of much low-frequency power in H_3 velocity, below ~ 4 mHz, whereas the large amount of high-frequency power (3–10 mHz) seen in the internetwork is not visible in the network. Another, less marked, area of inner wing brightening occurs around $x = 19$ Mm in the top panel. It likewise has more low-frequency and less high-frequency power than the areas with the darkest H-line profiles. Thus, the network has strong enhancement of low-frequency power, while the high-frequency power which characterizes H_3 oscillations in the internetwork is strongly suppressed. The amount of power in these two types of oscillation is comparable. The network has a mean oscillation amplitude of 1.7 km s^{-1} for the $f = 0$–5 mHz band, while the internetwork has a mean amplitude of 1.5 km s^{-1} for the $f = 4$–8 mHz band.

The horizontal extent of the blobs of power is generally larger than the pixel size ($\Delta x = 0.4$ Mm). Their size may be attributed to inherent spatial scales of the oscillation patterns and to smearing by seeing. Seeing also produces high-frequency noise in the power spectrum by rapidly moving small velocity features over the spectrograph slit. Such seeing fluctuations contain much higher frequencies than our sampling rate, so that the seeing power is aliased throughout the entire frequency range of our discrete Fourier transform. On the basis of coherence spectra (see § 3.4) we attribute most of the power above 10 mHz to such seeing noise. A pronounced example is the vertical column at $x = 30$ Mm in the Ca II power spectrum, which indicates the presence of a small network element with a distinct velocity signature. Such seeing-induced high-frequency noise is not prominent in the photospheric Fe I power spectrum because the spatial interference patterns of the solar p-modes are intrinsically more extended over the solar surface and also change during the observing time.

Figure 5 shows similar power spectra computed from intensity variations. The top panel again displays the temporal averages of the H-line profiles along the slit. The middle panel shows the spatial variation of power spectra computed from the H_3 intensity variations, i.e., from the intensity value of each H-line profile at the wavelength of its minimum. The bottom panel shows power spectra for the H-index, which is the integrated intensity in a 0.09 nm wide band around the H-core (cf. Fig. 1 and Table 1). It is representative of solar spectroheliograms and filtergrams (e.g., Sivaraman & Livingston 1982; Damé et al. 1984; Damé & Martić 1987), and also of the stellar

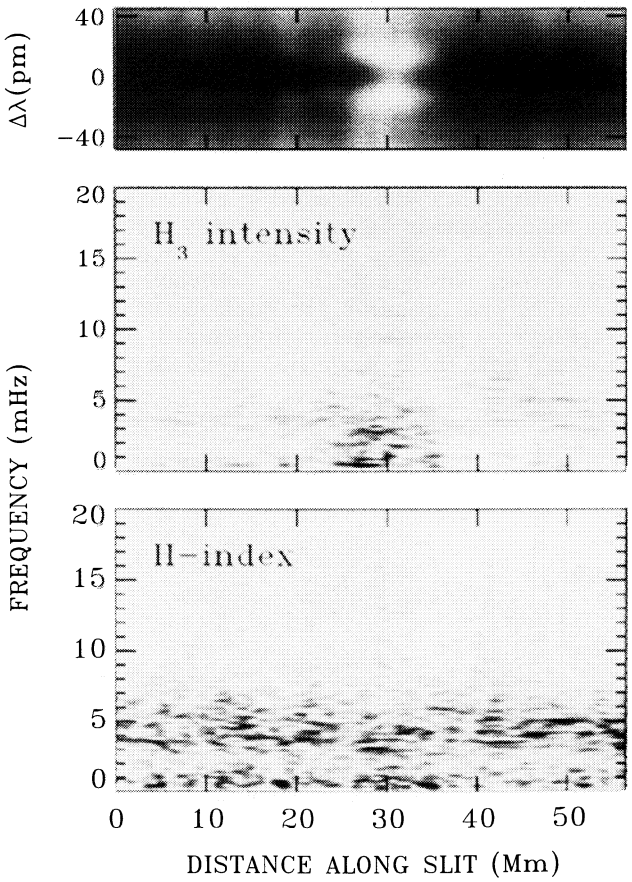

FIG. 5.—The spatially resolved power spectra of intensity fluctuations for H_3 (*middle panel*) and the H-index (*bottom panel*) are shown. The H-index is the intensity of the 0.09 nm wide band around the H core indicated in Fig. 1. The coding and the top panel are the same as in Fig. 4.

activity measurements made with the Mount Wilson photometer (Vaughan, Preston, & Wilson 1978; Oranje 1983).

Both power spectrum panels of Figure 5 differ from the Ca II H_3 Doppler shift panel in Figure 4. In the network, the H_3 intensity variations closely follow the H_3 velocity fluctuations. In the internetwork, however, there is much less high-frequency H_3 intensity power than H_3 velocity power. This striking difference is also seen in the chromospheric (k, ω) diagrams of Cram (1978). Cram made no distinction between network and internetwork, but our Figures 4 and 5 show that the absence of H_3 intensity power compared to H_3 velocity power is a property of the internetwork 3 minute oscillations.

The H-index panel contains much power in the $f = 3$–7 mHz band, without clear distinction between network and internetwork. The H-index power within this band is reminiscent of the p-mode strip in the Fe I velocity power panel of Figure 4, but it extends to higher frequencies. This high-frequency power is the Fourier representation of the wing whiskers present in Ca II H and K spectrograms (Beckers & Artzner 1974; Rutten & Uitenbroek 1991).

There is a small amount of internetwork power at very low frequencies in both H_3 panels which is perhaps due to residual effects of the measurement process. In contrast, the H-index panel contains much more power at the lowest frequencies ($f < 2$ mHz), without clear distinction between network and internetwork and with small spatial extent of the power blobs. Since the H_3 core does not show power at these frequencies, its source must be the inner wings of the H line, and it must therefore be of photospheric rather than chromospheric origin. Similar low-frequency power in the Ca II H-line wing was noted by Cram (1978), who tentatively attributed it to gravity waves (see also Schmieder 1976 and Deubner & Fleck 1989). It is presumably related to the so-called K0-continuum discussed by Suemoto et al. (1990).

Figure 6 shows the spatially averaged Ca II H_3 velocity power spectra. They were obtained by averaging the columns of the middle panel in Figure 4 separately over the network and internetwork regions along the slit. These mean power spectra further illustrate the large differences in oscillatory behavior between magnetic and nonmagnetic regions. The average network power spectrum drops rapidly for frequencies above $f = 4$ mHz, the approximate value of the acoustic cutoff frequency in the temperature minimum region, while the internetwork power increases at this frequency. Note that there is no distinct peak at 4 mHz frequency, as is the case in the power spectra of Deubner & Fleck (1990) for the Ca II infrared lines and of Kneer & von Uexküll (1986) for Hα. We discuss this distinction below (§ 4). Note also that the power level at very high frequencies is nearly the same for both regions, suggesting that there is no difference which might be present if seeing-induced motions and small-scale structures had conspired to produce differential enhancement of high-frequency power. Finally, we note that the three low-frequency peaks of the network spectrum lie at periods of ~1100 s, 550 s, and 400 s, respectively. We doubt that these represent selective modes of network oscillation.

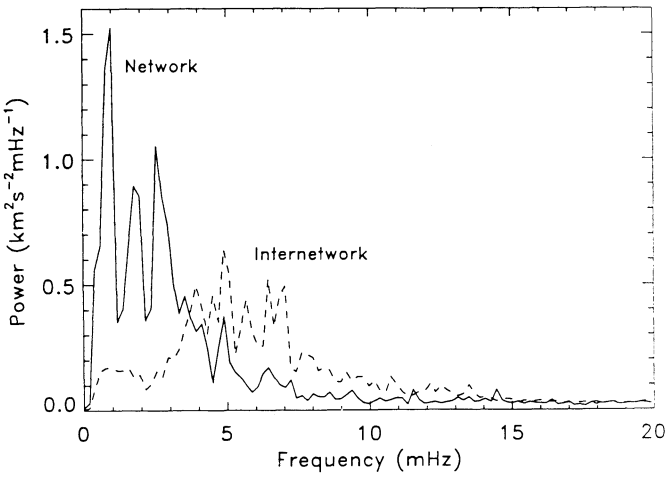

FIG. 6.—Velocity power spectra are shown for the Ca II H_3 excursions, with separate spatial averaging over the network (*solid curve*) and internetwork (*dashed curve*) regions along the slit.

3.4. *Phase and Coherence Spectra*

Phase and coherence spectra of oscillations provide information on the propagation characteristics of waves with height in the solar atmosphere. The 3 minute internetwork oscillations of the lower chromosphere as measured from the Ca II infared lines are highly coherent with the oscillations in the underlying photosphere (Lites et al. 1982; Deubner & Fleck 1990), indicating that internetwork disturbances of the chromosphere are directly related to the photospheric oscillations underneath. We demonstrate in this section that this is not the case for the network region in our data.

Figure 7 presents phase difference and phase coherence spectra for two line pairs. The upper panels show velocity phase differences, respectively for the network (top panels) and the internetwork (middle panels). The bottom panels present spatially averaged phase coherence spectra, also split between network (solid curves) and internetwork (dashed curves). The left hand panels show the phase delay and coherence between the photospheric Fe I 396.68 nm line and Ca I 422.67 nm, which forms in the vicinity of the temperature minimum. The right-hand panels show the phase delay and coherence between Ca I 422.67 nm and the chromospheric Ca II H_3 core. The phase difference at high frequency provides height of formation estimates which suggest that the lines in each pair are separated by ~400 km in response height (Table 1).

These diagrams were constructed as follows. Phase differences were computed for each line pair as a function of frequency for every spatial sample along the slit. We then obtained per frequency the geometric mean of the amplitudes of the two pertinent oscillation components for each line pair at each spatial position within equally sized spatial samples of network or internetwork. For both regions we built images representing oscillation amplitude versus phase difference and frequency. Finally, each frequency column of these images was normalized. This method permits visualization of the distribution of phase difference among spatial samples, either as a gray-scale image or as a graph in which only the highest amplitudes (typically the top 5%–7%) are displayed as one-bit images. The latter display is used for the phase difference panels of Figures 7 and 8. Its advantage over plotting spatially averaged curves is that it gives a direct impression of the scatter.

Phase coherence spectra provide a representation of phase persistence. Let

$$\tilde{v}_1(x, f) \equiv a_1(x, f) + ib_1(x, f) , \quad (1)$$

$$\tilde{v}_2(x, f) \equiv a_2(x, f) + ib_2(x, f) , \quad (2)$$

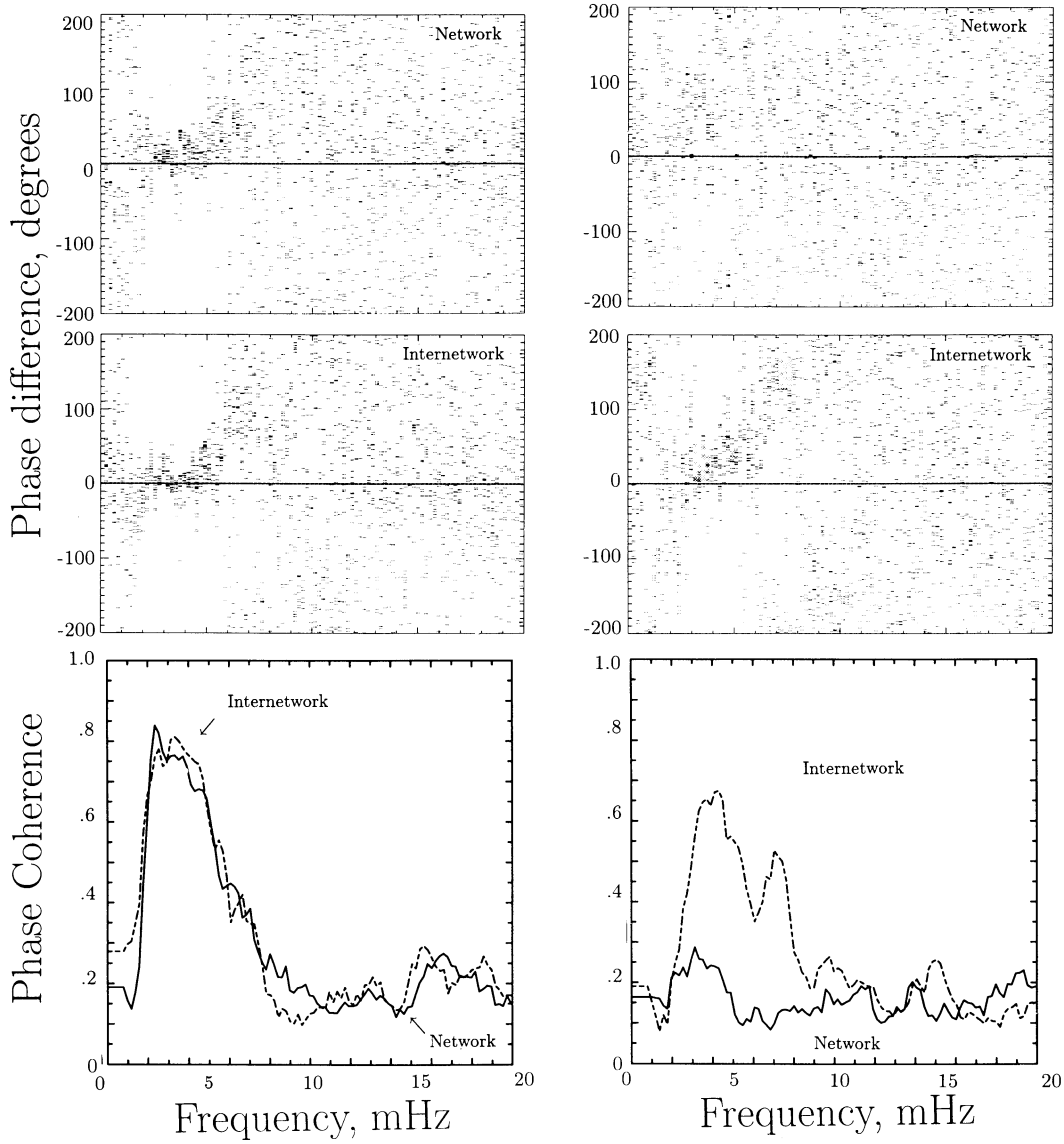

FIG. 7.—The variation of the velocity ($V-V$) phase difference and coherence C^2 between the Doppler excursions of two line pairs is shown as a function of frequency. The panels on the left correspond to phase differences and coherence between the pair Fe I 396.68 nm–Ca I 422.67 nm, and the panels on the right correspond to the pair Ca I 422.67 nm–Ca II H_3. The upper and middle panels show phase differences for the network and internetwork, respectively. Positive phase difference indicates that the velocity excursions in the first line lead those of the second. The bottom panels show phase coherence for the corresponding line pairs. The coherence is computed for a 1.75 mHz running average in frequency, separately for equal spatial averages of network (*solid curves*) and internetwork (*dashed curves*).

represent the discrete Fourier transforms of the time series $v_1(x, t)$ and $v_2(x, t)$ of Doppler velocities measured from lines 1 and 2, respectively. Here, x represents position along the slit, t time, and f Fourier frequency. The cross-power spectrum of the two time series is

$$\tilde{v}_1(x, f)\tilde{v}_2^*(x, f) \equiv c(x, f) + id(x, f) . \quad (3)$$

In the above definitions a, b, c, and d designate real numbers. The coherence spectrum $C(x, f)$ is defined by (Edmonds & Webb 1972):

$$C^2 \equiv \frac{\langle \tilde{v}_1 \tilde{v}_2^* \rangle [\langle \tilde{v}_1 \tilde{v}_2^* \rangle]^*}{\langle \tilde{v}_1 \tilde{v}_1^* \rangle \langle \tilde{v}_2 \tilde{v}_2^* \rangle} = \frac{\langle c^2 \rangle + \langle d^2 \rangle}{\langle a_1^2 + b_1^2 \rangle \langle a_2^2 + b_2^2 \rangle} , \quad (4)$$

where angle brackets represent averaging over frequency. Without averaging, the coherence is unity; that is, the difference in the phase of oscillation of the two lines at a given spatial position is a unique and definite quantity for each discrete Fourier frequency, regardless of their relative oscillation amplitudes at that frequency. We adopt a smoothing width of 9 frequency intervals in the discrete Fourier transform domain ($\Delta f = 1.75$ mHz); the coherence C^2 shown in Figures 7 and 8 is therefore displayed as constant for $f < 1$ mHz. The computed coherence spectra are not highly sensitive to the width of this smoothing function. In any case, phase coherence is a relative measure. The curves in the bottom panels of Figure 7 represent the average of the coherence over the spatial samples of network and internetwork. The level of the phase coherence at the highest frequencies, where the observed signal is surely dominated by noise, indicates the basal level at which oscillations measured in the two lines are fully incoherent. The

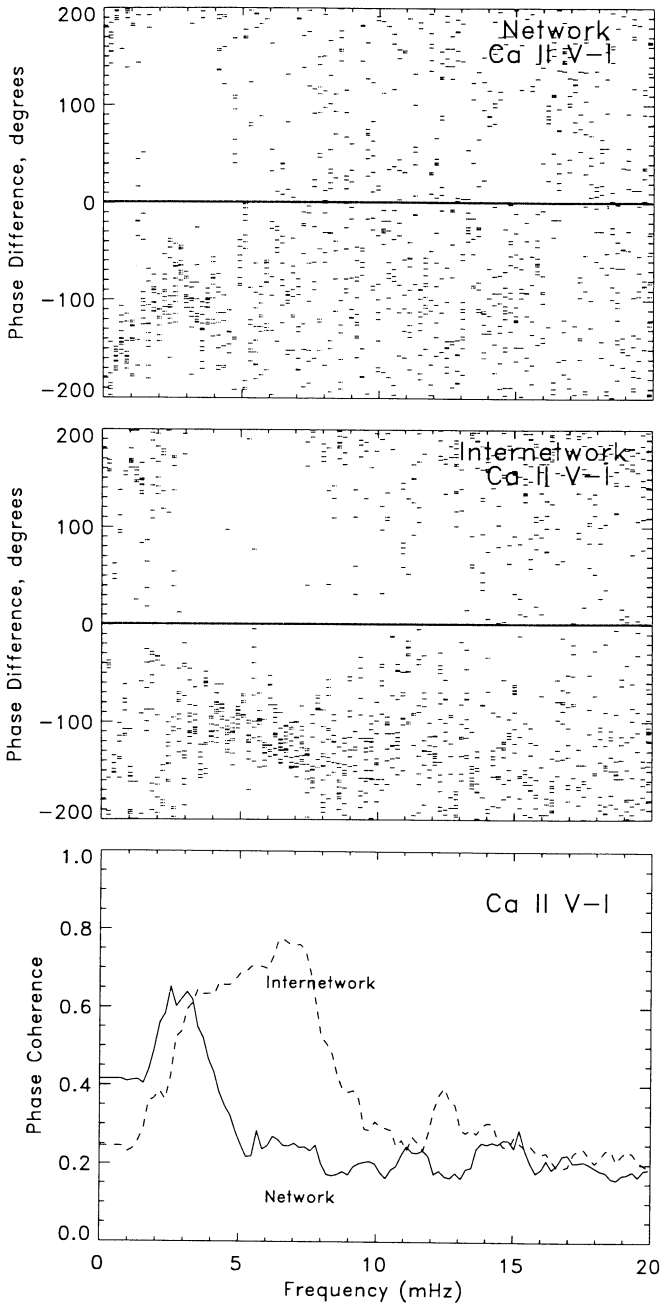

FIG. 8.—The variation of the $V-I$ phase difference and coherence C^2 between Dopper excursions and intensity variations for Ca II H_3 is given as a function of frequency. The upper and middle panels show phase differences for the network and internetwork, respectively. Positive phase difference implies that blueshift leads brightening. The coherence is computed using a 1.75 mHz running average in frequency, separately for equal spatial averages along the slit of network (*solid curves*) and internetwork (*dashed curves*).

bottom panels of Figure 7 indicate that this is the case for $f > 10$ mHz for both line pairs.

It is also possible to calculate the coherence as a spatial persistence of phase (e.g., Fleck 1991). However, we prefer the frequency averaging described above because it is not directly influenced by spatial resolution, seeing, and the intrinsic spatial variation of the phase difference. This attribute is especially important for observational studies at high angular resolution. Note that the above definition of coherence may be applied equally to a single time series.

The left-hand panels in Figure 7 indicate that the *p*-mode oscillations are coherent between the photosphere and temperature minimum for both the network and internetwork regions. The phase spectra show the familiar behavior of evanescent waves in the 5 minute band ($f = 2$–4 mHz) and indicate that there is progressively increasing vertical propagation for higher frequencies. This phase behavior is well known (Lites & Chipman 1979). The coherence spectra on the left show a very high degree of coherence within the 5 minute band and similar behavior for network and internetwork, illustrating that only slight differences in phase behavior exist between these two regions across the photosphere (Lites et al. 1982). The coherence is low, and the phase differences scatter widely for $f > 8$ mHz, indicating domination by noise.

The right-hand panels of Figure 7 demonstrate again that there is a marked difference between network and internetwork oscillations in the chromosphere. In the internetwork there remains considerable phase coherence over a broad frequency range ($f = 2$–8 mHz). The internetwork phase differences still show the familiar signatures of evanescent and propagating waves. In contrast, the network phase difference diagram (top, right-hand panel) has the appearance of nearly random scattering, except for a slight preference for positive phases in the *p*-mode region near 3 mHz. The bottom panel indicates that there is indeed no significant coherence between the network oscillations measured at these two heights, in particular for the low frequencies in which the chromospheric network oscillates with large power. We conclude that, in contrast to the internetwork oscillations, *the chromospheric oscillations observed in the network are not correlated with velocity fluctuations in the photosphere immediately underneath.*

Finally, we display $V-I$ (velocity versus intensity) phase difference and coherence spectra between H_3 and Dopplershift and intensity variations in Figure 8. We caution the reader that interpreting these diagrams is difficult since the response of the Ca II H core intensity to dynamical disturbances is not well known. In particular, the intensity and velocity responses may not be attributed to the same height in the atmosphere and they may change considerably with frequency (cf. Mein & Mein 1980). It will be necessary to study detailed numerical simulations of chromospheric dynamics including H and K line formation before such diagrams can be interpreted with confidence. We display $V-I$ here rather as enticement for such studies.

Figure 8 again shows large difference between the network and internetwork regions. the $V-I$ phase coherence (bottom panel) conforms to the Ca II power spectra in Figure 4 by showing increased coherence where the H_3 power is large. The network has high coherence between velocity and intensity fluctuations only at low frequencies, dropping off near $f = 4$ mHz. The phase differences are negative. Brightening leads upward motion by half a cycle at the lowest frequencies, the difference decreasing to $\sim 80°$ near $f = 3$ mHz. In contrast, the internetwork has low coherence and large phase difference scatter at low frequencies ($f < 3$ mHz), but high-frequency oscillations are present up to $f \approx 10$ mHz, perhaps even higher.

4. DISCUSSION

Our observations show very clearly that the chromospheric network participates in fluctuations with characteristic time

scales in excess of 5 minutes. The existence of such long period fluctuations has been noted before, but only with diagnostics which do not clearly demonstrate their chromospheric nature and which mix them with higher frequency oscillations. In this section we first compare our results with these earlier reports, and then discuss the nature of these slow variations.

4.1. *Comparison with Other Work*

4.1.1. Ca II H *and* K

Orrall (1966) measured displacements of the Ca II K line center from a 25 minute sequence of photographic spectrograms and was the first to report the presence of regular oscillations with periods up to 600 s in the network and up to 900 s in a plage. This range of periods is in agreement with the power spectrum of Figure 6. Liu & Sheeley (1971) measured intensity variations from K_{2V} spectroheliograms and found that the network oscillates regularly at 300 s, while the internetwork oscillates with a period of ~ 170 s. Taking their K_{2V} intensity as proxy for H_3 Doppler shift, we find that their value of 300 s corresponds to the shortest periods displayed by the network segment in our data (Fig. 4).

Cram (1978) derived (k, ω) diagrams from HIRKHAD (Beckers et al. 1972) spectrograms including the Ca II K line. He did not separate network and internetwork but states (in Cram et al. 1977) that the slit traversed very little of the chromospheric network. Indeed, his K-line velocity power spectrum has enhanced high-frequency and depressed low-frequency power, and his K-line $V-I$ phase difference spectrum[5] does not show the distinct approach toward $-\pi$ at the lowest frequencies seen in the top panel of Figure 8.

Damé et al. (1984) analyzed the intensity variations of a 52 minute sequence of Ca II K filtergrams taken with a 0.12 nm FWHM bandpass. Their two-dimensional display of power as a function of frequency and brightness contains poorly defined ridges of enhanced power at constant frequency for the brightest features within their field of view, which they ascribe to the calcium network. Comparison between Figures 4 and 5 shows that the long-period network oscillations which are so prominent in both H_3 velocity and H_3 intensity (the two middle panels) do not stand out at all in the H-index (bottom panel of Fig. 5). The latter panel could not have served as an indicator of network presence along the slit. The FWHM of the passband of Damé et al. was 30% wider than the full width of the H-index, but since it peaked at K_3 it may have given similar response. Comparison of the lower panels of Figure 5 clearly shows that much narrower bandwidth is required to measure the chromospheric network oscillations with certainty.

4.1.2. *The* Ca II *Infrared Lines*

The infrared lines of Ca II (hereafter IR) have also often been used as diagnostics of oscillations in the lower chromosphere. Low-frequency disturbances associated with the network have been observed in these lines, but with confused signatures which make interpretation difficult.

Lites et al. (1982) concentrated on differences between internetwork and network for frequencies at which the p-modes are evanescent ($f = 2.5$–5 mHz) but, for $f < 2$ mHz, their Figures 8 and 9 contain also substantial network-internetwork differences in $V-I$ phase delay between Ca II 849.8 nm and Ca II 854.2 nm. These differences are opposite between the two lines. In the internetwork, the low-frequency velocity perturbations appear to lead the intensity fluctuations of Ca II 854.2 nm while the reverse is the case for Ca II 849.8 nm.

Deubner & Fleck (1990) performed a Ca II IR analysis similar to Lites et al. (1982), but they measured full spectral-line profiles (as we do here) so that the resulting line center intensity and Doppler variations suffer less from spread in response height (see Lites & Chipman 1979). Deubner & Fleck find that the velocity and intensity power spectra of Ca II 854.2 nm differ between network and internetwork. Both regions show a dominant power peak for evanescent p-modes at $f = 4$ mHz with a high-frequency tail (first found by Evans et al. 1963), but the network has considerably more power at frequencies around 2 mHz where IR line power spectra display a deep dip.

Our H_3 power spectra (Figs. 4–6) differ markedly from these Ca II IR power spectra in that they do not show such a prominent p-mode power peak at all. However, the broad-band H-index panel in Figure 5, in which lower atmosphere photons are mixed in with the H_3 intensity signal, resembles the power spectra of Deubner & Fleck. It also has a large p-mode peak at $f = 4$ mHz, a high-frequency tail and a deep dip around $f = 2$ mHz. This similarity implies that the IR Doppler shifts contain a significant contribution from the lower atmosphere, whereas the Doppler shifts of the H and K lines are set entirely in the chromosphere. Rutten & Uitenbroek (1991) also noted from the (k, ω) diagrams of Cram (1978) that the Ca II 854.2 nm line responds to the same layers of the atmosphere as the inner wings of the H and K lines. However, it should display some K_3 behavior as well because the Ca II IR line source functions are coupled with non–LTE-enhanced sensitivity to the H and K source functions (Uitenbroek 1989).

The same conclusion follows from comparison between our H_3 $V-I$ diagrams with the $V-I$ spectra for Ca II 854.2 nm in Figure 6 of Deubner & Fleck (1990). The phase differences in the latter are the same for network and internetwork whereas the upper panels of our Figure 8 display substantial difference, particularly at higher frequencies. The $V-I$ phase difference spectra show some commonality in that both the IR and H_3 $V-I$ phase difference spectra increase steeply from $-180°$ to about $-70°$ between 0 and 3 mHz. This rise is also present in Figure 9 of Lites et al. (1982). The IR and H_3 $V-I$ variations also share higher coherence in the network at low frequencies and a cross over to higher coherence in the internetwork at higher frequencies, but this behavior is far more pronounced for H_3 than for Ca II 854.2 nm. This confirms that the Ca II IR lines present a mixed diagnostic of the upper photosphere and low chromosphere, further complicating the already cloudy problem of interpretation of $V-I$ phase spectra.

Another confusing IR line property is that the weakest IR line (Ca II 849.8 nm) has anomalous response to fluctuations. Both its intensity and velocity response functions peak higher in the atmosphere than one would expect (for some frequencies they even peak at about the same height), which is unusual for lines in which scattering dominates (Mein 1964, 1966, 1971; Shine & Linsky 1974; Provost & Mein 1979; Mein & Mein 1980; Uitenbroek 1989; cf. Rutten & Uitenbroek 1991). Deubner & Fleck (1990) are puzzled by the absence of enhanced internetwork power around $f = 4$ mHz in their velocity power spectrum for this line (their Fig. 2), which they

[5] Note that Cram (1978) and others take downward velocity positive. We follow the opposite convention of Lites et al. (1982) and Deubner & Fleck (1990), with positive velocity corresponding to blueshift. For $V-I$ phase difference conversion, subtract 180°. Note also that Deubner (1990) plots $I-V$ rather than $V-I$.

ascribe to a nodal plane in the chromosphere. Above $f = 3$ mHz the Ca II 849.8 nm power spectrum resembles the H-index panel of Figure 5, which suggests a low formation height. However, at lower frequencies it contains significant enhancement of network over internetwork power which suggests response to higher layers. The $V-V$ phase differences between Ca II 849.8 nm and Ca II 854.2 nm also pose problems. Overall, they are very small, for which Deubner & Fleck invoke standing waves. The $V-V$ phase differences are positive in the internetwork, but in the network the Ca II 854.2 nm phases lag behind those of Ca II 849.8 nm by up to 15° at low frequencies. The latter differences are interpreted by Deubner & Fleck as evidence for magnetogravity waves that "fall" from canopies down into flux tubes.

In summary, the IR lines exhibit characteristics both of H_3-like chromospheric behavior and of H-index-like lower atmosphere behavior. We feel that the purely chromospheric dynamics observed in the Ca II H & K lines should be understood before speculating too much on the confused diagnostics presented by the Ca II IR lines. In particular, there is the possibility that the emission in these lines is so localized due to nonlinear dynamics of the chromosphere that standard formation estimates based on plane-parallel time-independent models are rendered fully unreliable (see Rammacher & Ulmschneider 1992).

4.1.3. Hα

Observations of Hα also suggest a difference in temporal fluctuations between the network and internetwork regions. Title (1966) noted a characteristic period of 550 s for the mean Doppler signal in Hα as measured over an area of 30 by 30 Mm. Bhatnagar & Tanaka (1972) measured intensity fluctuations at $\Delta\lambda = -0.05$ nm from the Hα line center and found that the network oscillates with periods around 300 s while the internetwork has higher frequency variations. Kneer & von Uexküll (1985) found fluctuations with periods above 450 s in sequences of Hα images, both on and off band. They identified these as belonging to network regions.

The more recent Hα MSDP observations of von Uexküll et al. (1989) clearly show differences in oscillatory character between network and internetwork. The velocity power spectra in their Figure 3 show a wide ($f = 3$–8 mHz) peak for the internetwork which is suppressed in the network, especially when only the brighter pixels are sampled. The network shows a single power peak at low frequency, corresponding to the Ca II H behavior in our Figure 4. However, the internetwork Hα intensity power spectrum shares the same low-frequency peak. In our Figure 5 it is absent in the internetwork parts of the H_3 panel, but it is present in the H-index panel. This indicates that Hα line-center intensity senses the lower atmosphere also (cf. Schoolman 1972). At low frequencies the Hα $V-I$ phase difference and coherence spectra roughly resemble the behavior in Figure 8 (Figs. 3*c* and 3*d* of Von Uexküll et al., after subtraction of 180° for velocity sign convection).

4.2. *The Nature of Long-Period Network Motions*

Visual inspection of their filtergram time sequences suggested to Kneer & von Uexküll (1985, 1986) that the low-frequency behavior of the network is due to stochastic motions of magnetic structures which are driven by the granulation and oscillations in the subphotosphere. Von Uexküll et al. (1989) found that the observed motions are insufficient to heat the active chromosphere, even after upward adjustment of their measured rms line shifts for Hα radiative transfer. They speculate that these motions indicate rearrangements of the magnetic field in the chromosphere, which then result in continuous localized heating through in situ resistive dissipation of the chromospheric magnetic field (cf. Parker 1988). This scheme is the opposite of the speculation by Deubner & Fleck (1990) that upward propagating (magneto-)gravity waves in the internetwork fall down in network flux tubes. Kneer & von Uexküll (1985) did not find ridges in the gravity wave domain of their (k, ω) diagrams, but such ridges are likely to be unobservable for gravity modes that are confined to isolated network structures.

Although the present observations are of limited duration, the periodic appearance of the slow network disturbances in Figure 2 and their apparent horizontal propagation in the same figure suggest that they represent a periodic phenomenon rather than a stochastic one. We have also found that the slow network oscillations are not directly related to the dynamics of the underlying atmosphere. Thus, these disturbances are either confined to the chromosphere or they are excited by photospheric events that take place at some horizontal distance from the locus of observation. Granular overshoot in the photosphere is a likely source of such chromospheric disturbances since granulation has the required small spatial scaling (1—2 Mm). The *p*-mode excursions are unlikely drivers because they do not have significant power at these low frequencies and because they are coherent over much larger areas. If they were the source of slow network disturbances, one would find higher phase coherence with the photospheric diagnostics than we observe.

The horizontal dimensions of the low-frequency network power blobs in the H_3 panels of Figures 4 and 5 are sufficiently large to be resolved in these observations. The observed oscillation amplitudes are subsonic, but we may well measure only a small component of the actual flows if they occur along inclined structures in "rosettes" (Beckers 1964). We also note that breaking gravity waves are expected to possess much larger horizontal than vertical velocities and may result in significant heating of the chromosphere because they can dissipate large amounts of energy even for small vertical velocities (Mihalas & Toomre 1981). Discrimination between this possibility of upward magneto-gravity wave energy transport along rosette structures and downward energy transport as suggested by Deubner & Fleck (1990) can be tested by observations of purely chromospheric spectral lines. If the observed motions represent flux rearrangements as suggested by von Uexküll et al. (1989), the resistive dissipation of the magnetic stresses would occur on unobservably small scales. Such rearrangements require only modest large-scale motions.

Long-period disturbances have also been observed in the *active* chromosphere, and these may be related to the long-period network oscillations. Beckers & Schultz (1972) found that the oscillation frequency of sunspot penumbrae decreases by more than a factor of 2 from the inner to the outer edges. Lites (1988) found similar behavior in a number of sunspots, where frequencies in the inner penumbra are typically 4 mHz and decrease to below 1.5 mHz at the outer edge. He suggested that the disturbances are related to the minus modes of Nye & Thomas (1974), in which both gravity and magnetic field contribute to the restoring force. Just as for the long-period network disturbances, the mechanism causing penumbral oscillations is not understood. However, the fact that these phenomena have similar periods and both occur in more

strongly magnetized regions of the solar chromosphere suggests that one should look for common mechanisms. As noted by Lites (1992), long-period penumbral oscillations may be associated with photospheric 5 minute oscillations, or they may be connected with the quasi-periodic fluctuations in the Evershed flow observed by Shine et al. (1990).

A final speculation concerns the stellar Wilson-Bappu effect, which statistically relates stellar luminosity and Ca II H and K line widths (Wilson & Bappu 1957; Linsky 1980). Figures 4 and 5 show variation in the temporally averaged Ca II H line profiles along the small segment of network along the slit. The separation of the H_{2V} and H_{2R} emission peaks is larger at the left and right than in the middle of the network segment. There is also variation at similar length scales in the H_3 power spectra in the middle panels. Perhaps there is a relation between the Wilson-Bappu width and the properties of these long-period network oscillations.

5. CONCLUSIONS

We draw the following conclusions from our observations and from our comparisons with previous work:

1. The chromospheric network participates in long-period oscillations ($f < 3$ mHz) with modest amplitudes (1–2 km s^{-1}).
2. Slow network oscillations are not correlated with oscillations in the layers immediately underneath, unlike internetwork regions.
3. Ca II H_3 and K_3 provide diagnostics of the network chromosphere which are reasonably restricted to chromospheric layers.
4. The Ca II IR lines are less clean diagnostics of chromospheric dynamics, due to substantial contamination by lower layers.
5. Our observations confirm earlier inferences from Ca II H and K, the Ca II IR lines and Hα that chromospheric brightenings correlated with downward motion at the lowest frequencies, progressing toward somewhat less than a one-fourth-cycle delay between brightening and upward motion at $f = 3$ mHz.

These slow network oscillations are of obvious interest in the context of the chromospheric energy balance and the magnetic structuring of the outer atmosphere. Identifying their nature is a first goal of future research. A high priority is to acquire long duration spectrogram sequences with two-dimensional coverage of the chromospheric network in order to search for photospheric drivers of horizontally propagating low-frequency waves in the chromosphere. In addition, observations of network oscillations at varying limb distances are needed to determine whether these motions have significant horizontal components and may also help to establish whether the waves are transverse or longitudinal to the magnetic field.

Another venture of considerable interest in this context is to study these phenomena with theoretical radiation-(magneto)-hydrodynamics simulations (see Carlsson & Stein 1992). We have pointed out above that interpreting variations of the Ca II H and K and IR lines cannot rely on simple height of formation estimates but requires detailed non-LTE line formation modeling taking these dynamical phenomena into account. Conversely, it will be very useful to apply the diagnostics that we have displayed above to such simulation results. In particular, interpreting $V-I$ phase difference behavior with guidance from numerical simulations in the form of similar representations may avoid pitfalls and turn out to be worthwhile.

We thank the observing staff of the National Solar Observatory/Sunspot for assistance in gathering these observations. We thank P. Judge for comments on the manuscript. We also thank the referee for several useful suggestions and a critique that helped us improve the presentation of this paper considerably. B. W. L. recognizes support for this work from NASA Grant SR&T 170-38-53-30. R. J. R. acknowledges travel support from NATO (CRG 900229). W. K. acknowledges support by NASA through grant NAGW 1568.

REFERENCES

Athay, R. G. 1970, Sol. Phys., 11, 347
Beckers, J. M. 1964, Ph.D. thesis, University of Utrecht (AFCRL Environmental Res. Paper, No. 49)
Beckers, J. M., & Artzner, G. 1974, Sol. Phys., 37, 309
Beckers, J. M., Mauter, H. A., Mann, G. R., & Brown, D. R. 1972, Sol. Phys., 25, 81
Beckers, J. M., & Schultz, R. B. 1972, Sol. Phys., 27, 61
Bhatnagar, A., & Tanaka, K. 1972, Sol. Phys., 24, 87
Biermann, L. 1946, Naturwissenschaften, 33, 118
Bruls, J. H. M. J., & Rutten, R. J. 1992, A&A, 265, 257
Carlsson, M., & Stein, R. F. 1992, ApJ, 397, L59
Cram, L. E. 1974, Sol. Phys., 37, 75
———. 1978, A&A, 70, 345
Cram, L. E., Brown, D. R., & Beckers, J. M. 1977, A&A, 57, 211
Cram, L. E., & Damé, L. 1983, ApJ, 272, 355
Damé, L., Gouttebroze, P., & Malherbe, J.-M. 1984, A&A, 130, 331
Damé, L., & Martić, M. 1987, ApJ, 314, L15
Deubner, F.-L. 1990, in IAU Symp. 138, The Solar Photosphere: Structure, Convection, and Magnetic Fields, ed. J.-O. Stenflo (Dordrecht: Kluwer), 217
Deubner, F.-L., & Fleck, B. 1989, A&A, 213, 423
———. 1990, A&A, 228, 506
Edmonds, F. N., & Webb, C. J. 1972, Sol. Phys., 22, 276
Evans, J. W., Michard, R., & Servajean, R. 1963, Ann d'Astrophys., 26, 368
Fleck, B. 1991, Ph.D. thesis, University of Würzburg
Frazier, E. N. 1968, ApJ, 152, 557
Giovanelli, R. 1975, Sol. Phys., 44, 299
Giovanelli, R. G. 1974, Sol. Phys., 37, 301
Kneer, F., & von Uexküll, M. 1985, A&A, 144, 443
———. 1986, A&A, 155, 178
Kuperus, M. 1969, Space Sci. Rev., 9. 713
Linsky, J. L. 1980, ARA&A, 18, 439
Lites, B. W. 1985, in Proc. MPA/LPARL Workshop, Theoretical Problems in High-Resolution Solar Physics, Max-Planck-Institut für Physik und Astrophysik MPA No. 212, ed. H. U. Schmidt (München: MPA), 273
———. 1988, ApJ, 334, 1054
———. 1992, in Sunspots: Theory and Observations, ed. N. O. Weiss & J. H. Thomas (Dordrecht: Kluwer), 261
Lites, B. W., & Chipman, E. G. 1979, ApJ, 231, 570
Lites, B. W., Chipman, E. G., & White, O. R. 1982, ApJ, 253, 367
Lites, B. W., Scharmer, G. B., & Skumanich, A. 1990, ApJ, 355, 329
Lites, B. W., & Thomas, J. H. 1985, ApJ, 294, 682
Liu, S. Y., & Sheeley, N. R. 1971, Sol. Phys., 20, 282
Liu, S.-Y., Skumanich, A. 1974, Sol. Phys., 38, 105
Mein, N., & Mein, P. 1980, A&A, 84, 96
Mein, P. 1964, Comptes Renduz, 258, 819
———. 1966, Ann. d'Astrophys., 29, 153
———. 1971, Sol. Phys., 20, 3
Mein, P., Mein, N., Malherbe, J. M., & Damé, L. 1987, A&A, 177, 283
Mihalas, B. W., & Toomre, J. 1981, ApJ, 249, 349
Moore, C. E., Minnaert, M. G. J., & Houtgast, J. 1966, The Solar Spectrum 2935 Å to 8770 Å. 2d Rev. of Rowland's Preliminary Table of Solar Spectrum Wavelengths, NBS Monog. 61 (Washington, DC: NBS)
Musman, S., & Rust, D. M. 1970, Sol. Phys., 13, 261
Noyes, R. W. 1967, in IAU Symp. 28, Aerodynamic Phenomena in Stellar Atmospheres, ed. R. N. Thomas (London: Academic), 293
Noyes, R. W., & Leighton, R. B. 1963, ApJ, 138, 631
Nye, A. H., & Thomas, J. H. 1974, Sol. Phys., 38, 399
Oranje, B. J. 1983, A&A, 122, 88
Orrall, F. Q. 1966, ApJ, 143, 917
Parker, E. N. 1988, ApJ, 330, 474
Provost, J., & Mein, 1979, Sol. Phys., 64., 43
Rammacher, W., & Ulmschneider, P. 1992, A&A, 253, 586

Rutten, R. J., & Uitenbroek, H. 1991, Sol. Phys., 134, 15
Schmieder, B. 1976, Sol. Phys., 47, 435
Schoolman, S. A. 1972, Sol. Phys., 22, 344
Schwarzschild, M. 1948, ApJ, 107, 1
Shine, R., Smith, K., Tarbell, T., Title, A., & Scharmer, G. 1990, BAAS, 22, 878
Shine, R. A., & Linsky, J. L. 1974, Sol. Phys., 39, 49
Sivaraman, K. R., Livingston, W. C. 1982, Sol. Phys., 80, 227,
Stenflo, J.-O. 1989, Astron. Astrophys. Rev., 1, 3
Suemoto, Z., Hiei, E., & Nakagomi, Y. 1990, Sol. Phys., 127, 11
Title, A. M. 1966, A Study of Velocity Fields in the Hα Chromosphere by Means of Time-Lapse Doppler Movies (Pasadena: California Inst. of Technology)
Uitenbroek, H. 1989, A&A, 213, 360
Ulmschneider, P., Priest, E. R., & Rosner, E. R. eds., 1991, Proc. Internat. Heidelberg Conf., Mechanisms of Chromospheric and Coronal Heating (Berlin: Springer)
Vaughan, A. H., Preston, G. W., & Wilson, O. C. 1978, PASP, 90, 267
von Uexküll, M., Kneer, F., Malherbe, J. M., & Mein, P. 1989, A&A, 208, 290
Wilson, O. C., & Bappu, M. K. V. 1957, ApJ, 125, 661
Wilson, P. R., Rees, D. E., Beckers, J. M., & Brown, D. R. 1972, Sol. Phys., 25, 86
Woods, D. T., & Cram, L. E. 1981, Sol. Phys., 69, 233